Journal of Computer and Communications, 2023, 11, 149-164
https://www.scirp.org/journal/jcc
ISSN Online: 2327-5227
ISSN Print: 2327-5219

Estimating Brain Functional Networks Based on Spatiotemporal Higher-Order Correlations for Autism Identification

Mengxue Pang[1], Limei Zhang[2], Xueyan Liu[1], Tinglin Zhang[3], Shufeng Zhou[1*]

[1]School of Mathematics Science, Liaocheng University, Liaocheng, China
[2]School of Computer Science and Technology, Shandong Jianzhu University, Jinan, China
[3]School of Information Engineering, Yancheng Institute of Technology, Yancheng, China
Email: pangmengxue_lemon@163.com, zhanglimei22@sdjzu.edu.cn, lculxy@126.com, ztlyoyo@ycit.edu.cn, *zhoushufeng@lcu.edu.cn

How to cite this paper: Pang, M.X., Zhang, L.M., Liu, X.Y., Zhang, T.L. and Zhou, S.F. (2023) Estimating Brain Functional Networks Based on Spatiotemporal Higher-Order Correlations for Autism Identification. *Journal of Computer and Communications*, **11**, 149-164.
https://doi.org/10.4236/jcc.2023.118011

Received: July 29, 2023
Accepted: August 27, 2023
Published: August 30, 2023

Abstract

Brain functional network (BFN) has become an important tool for the analysis and diagnosis of brain diseases, and how to build a high-quality BFN based on resting-state functional magnetic resonance imaging (rs-fMRI) has become a growing concern in the neuroscience community. Although some methods have been proposed to construct a high-quality BFN, they only encode the spatial characteristics of the ROIs, ignoring the temporal characteristics. As a result, it becomes challenging to accurately capture the true state of the brain. To address this problem, we propose a novel method to construct a higher-order BFN, considering both temporal and spatial domain characteristics. In particular, we get the characteristics of the temporal domain by differentiating the rs-fMRI signal itself, and then we integrate the information of the spatial domain and temporal domain to build a high-order BFN. To evaluate the proposed method, we conduct our experiments on ABIDE database to identify subjects with Autism Spectrum Disorder (ASD) from normal controls. Experimental results show that our method can achieve higher performance than baseline methods.

Keywords

Functional MRI, HOFN, Difference, Autism Spectrum Disorder

1. Introduction

Autism spectrum disorder (ASD) is a serious developmental disorder, characterised by major symptoms such as social withdrawal, impaired communication

disorders and repetitive behaviors [1] [2] [3]. In 2021, the latest data released by the Centers for Disease Control and Prevention (CDC) in the United States showed that the incidence of ASD among American children has reached 1 in 44 [4]. The pathogenesis of autism is still unclear, which brings a heavy burden to families and society. Currently, early intervention for ASD is recognized as an effective way to treat ASD and significantly improve patients' quality of life.

Resting-state functional magnetic resonance imaging (rs-fMRI) is a non-invasive and non-intrusive neuroimaging technique that typically captures the spontaneous brain activity of subjects not receiving external stimuli by measuring the blood-oxygen-level-dependent (BOLD) signals of the brain [5] [6]. The rs-fMRI technique holds significant value for the diagnosis and treatment of brain disorders, such as ASD, in clinical research. The construction of the brain functional network (BFN) based on rs-fMRI provides essential support for early diagnosis of ASD [7] [8]. Despite its importance, how to construct a high-quality BFN remains a critical issue of concern among researchers.

Recently, researchers have proposed various methods to construct BFN (such as Pearson's correlation (PC) [9], sparse representation (SR) [10], and group-sparsity representation (GSR) [11]). Although these methods have been widely applied, they are limited in their ability to capture only low-order relationships between brain regions of interest (ROIs) and thus are not capable of capturing more complicated interactions within the brain.

To capture the complex interactions within the ROIs, researchers have proposed some advanced BFN estimation methods and successfully applied them in the early diagnosis of brain diseases. Zhao *et al.* utilized the multi-level high-order BFN (HoFN) based on PC for diagnosing ASD [12]; Zhang *et al.* examined a method of constructing high-order BFNs through two consecutive correlation operations, which was employed for the diagnosis of abnormalities in Mild Cognitive Impairment (MCI) [13]. Chen *et al.* developed the HoFN estimation method based on sliding window and applied it to the classification of MCI [14]; and Su *et al.* proposed a correlation-preserving embedding method for constructing high-order BFNs (*i.e.*, HoFN_cope) and applied it to the classification and identification of MCI [15]. However, the construction of these high-order BFNs directly uses the row or column of the adjacency matrix of the low-order BFN as the feature vectors of the ROIs, which only considers the spatial dimension of features (the relationship between ROIs), while ignoring the temporal characteristics of individual ROIs.

To address this issue, we propose a novel method for constructing a high-order BFN. Specifically, we encode the temporal characteristics of ROIs by calculating the differencing of time series data, and then integrate the temporal features into the process of constructing a higher-order BFN. Compared with existing methods for constructing BFN, our proposed method has the following characteristics:

1) It is a high-order approach for constructing BFN, which can model more complex structures between ROIs and accurately reflect more intricate interac-

tions in the brain.

2) The BFN we built not only integrates spatial characteristics between ROIs, but also includes temporal characteristics. By combining characteristics from both dimensions, the resulting BFN more accurately reflects the true state of the brain.

3) Last but definitely not least, the method we proposed is highly flexible and does not conflict with traditional approaches to BFN construction. We tested our method on the ABIDE dataset to identify ASD. The results demonstrated that our method outperformed the baseline method.

The rest of this paper is organized as follows. In Section 2, we first introduce the pipeline of data preparation and then review the related works. After that, we present our BFN estimation model. In Section 3, we describe the experimental setting and experimental results. In Section 4, we investigate the effect of the BFN modelling parameters. Finally, we conclude this paper in Section 5.

2. Materials and Methods

In this section, we describe the data preparation (including data acquisition and preprocessing), and BFN construction methods (including the baseline and the proposed methods).

2.1. Data Acquisition and Preprocessing

In this paper, we adopted a targeted strategy to avoid overfitting. Specifically, we selected the largest and second-largest sites, New York University (NYU) and the University of Michigan (UM), from the ABIDE[1] dataset to validate the effectiveness of the model we proposed. The demographic information of these subjects is shown in **Table 1**. Specifically, for the NYU site, which comprises a total of 184 subjects, including 105 normal controls and 79 ASDs, and all the rs-fMRI data are acquired using a standard echo-planar imaging sequence on a clinical routine 3.0 Tesla Allegra scanner, and the imaging parameters are set as follows: TR/TE is 2000/15 ms with 180 volumes, and the number of the slice is 33. For UM site, there are 145 subjects, including 77 healthy controls and 68 ASDs. The rs-fMRI data are obtained by 3.0 Tesla Verio. Since we get the rs-fMRI, rs-fMRI data are further preprocessed by the Data Processing Assistant for Resting state fMRI toolbox (DPARSF) [16]. Specifically the preprocessed pipeline primarily consists of the following steps: 1) volume slicing and correction of head motion; 2) nuisance signals regression (including ventricle, white matter signals as well as the high-order effect of head motion described by Friston 24-parameters model); 3) registration to MNI space; and 4) temporal filtering (0.01 - 0.1 Hz) using both a linear downtrend and fast Fourier transform methods. Then, the brain is parcellated into 116 ROIs based on the AAL atlases [17]; Finally, the mean time series extracted from all these ROIs are assembled into the data matrix $X_1 \in R^{175\times116}$ ($X_2 \in R^{295\times116}$).

[1]http://fcon_1000.projects.nitrc.org/indi/abide

Table 1. Demographic and clinical information of subjects in the ABIDE dataset. Values are reported as mean ± standard deviation. M/F: Male/Female; FIQ: Full-Scale Intelligence Quotient; VIQ: Verbal Intelligence Quotient; PIQ: Performance Intelligence Quotient.

Datasets	Class	Gender (M/F)	Age (Years)	FIQ	VIQ	PIQ
YU	ASD	68/11	14.51 ± 6.23	107.92 ± 3.15	105.81 ± 1.23	108.81 ± 2.10
	NC	79/26	15.80 ± 3.23	113.15 ± 2.45	113.13 ± 1.15	115.07 ± 2.08
UM	ASD	58/10	13.13 ± 2.14	105.46 ± 17.28	---	---
	NC	59/18	14.79 ± 3.51	108.12 ± 9.80	---	---

2.2. Related Works

2.2.1. Pearson's Correlation

As previously mentioned, PC is the simplest and most popular method for constructing BFN. Denote $x_i \in R^T$ as the rs-fMRI time series extracted from the *i-th* ROI, in which T represents the number of time points in each series. The weight between the *i-th* and *j-th* ROIs based on PC is defined as follows:

$$W_{ij} = \frac{\left(x_i - \bar{x}_i\right)^T \left(x_j - \bar{x}_j\right)}{\sqrt{\left(x_i - \bar{x}_i\right)^T \left(x_i - \bar{x}_i\right)} \sqrt{\left(x_j - \bar{x}_j\right)^T \left(x_j - \bar{x}_j\right)}} \tag{1}$$

where $\bar{x}_i \in R^T$ represents the mean vector that corresponds to *i-th* ROI. By re-defining $x_i \triangleq \left(x_i - \bar{x}_i\right) \Big/ \sqrt{\left(x_i - \bar{x}_i\right)^T \left(x_i - \bar{x}_i\right)}$, Equation (1) can be simplified into $W_{ij} = x_i^T x_j$, which corresponds to the solution of the following optimization problem:

$$\min_{W_{ij}} \sum_{ij}^{N} \left\| x_i - W_{ij} x_j \right\|^2 \tag{2}$$

According to a previous work [18], Equation (2) can be equivalently transformed into the following matrix form:

$$\min_{W} \left\| W - X^T X \right\|_F^2 \tag{3}$$

where $X = \left[x_1, x_2, \cdots, x_N\right] \in R^{T \times N}$ is the rs-fMRI time series, $W \in R^{N \times N}$ denotes the estimated BFN, and $\left\| \cdot \right\|_F$ represents the F-norm of a matrix.

In general, BFN constructed using PC method is a densely connected graph, meaning that all vertices are fully connected by edges. In practical applications, a threshold approach is commonly employed to sparsify the PC-based BFN by eliminating weak connections.

2.2.2. Sparse Representation

Despite the popularity of PC, it can only capture the full correlation between two ROIs. Sparse representation (SR) is a statistical method used to model partial correlation by regressing the confounding effects of other ROIs. The mathematical model of SR is expressed as follows:

$$\min_{W_{ij}} \sum_{i=1}^{N} \left(\left\| x_i - \sum_{j \neq i} W_{ij} x_j \right\|^2 + \lambda \sum_{j \neq i} \left| W_{ij} \right| \right) \tag{4}$$

Equivalently, it can be expressed in the following matrix form:

$$\begin{aligned} &\min_{W} \left\| X - XW \right\|_F^2 + \lambda \left\| W \right\|_1 \\ &\text{s.t.} \quad W_{ii} = 0, \forall i = 1, \cdots, N \end{aligned} \tag{5}$$

where $\left\| \cdot \right\|_1$ represents the L_1-norm of a matrix. To avoid a trivial solution, we employ the constraint that $W_{ii} = 0$. λ is a regularized parameter used to balance the first and second terms.

2.2.3. Group-Sparsity Representation

Both SR and PC estimate BFN one by one, without considering the potential relationship or shared structure among BFNs from different subjects. Recently, Wee *et al.* proposed GSR by introducing an $L_{2,1}$-norm ($\left\| \cdot \right\|_{2,1}$) regularization term to the BFN estimation model, aiming to address this issue. Specifically, the BFN estimation based on GSR can be expressed as:

$$\min_{W_n} \sum_{i=1}^{s} \left(\frac{1}{2} \left\| x_n^i - X_{\_n}^{\ i} w_n^i \right\|^2 + \lambda \left\| W_n \right\|_{2,1} \right), n = 1, 2, \cdots, N \tag{6}$$

where x_n^i represents the rs-fMRI time series of the *n*-th ROI for the *i*-th subject. $X_{\_n}^{\ i} = \left[x_1^i, \cdots, x_{n-1}^i, x_{n+1}^i, \cdots, x_N^i \right]$ represents the data matrix of the *i*-th subject, with the *n*-th ROI removed. w_n^i is the weight vector that denotes the influence of other ROIs on the *n*-th ROI for the *i*-th subject, $W_n = \left[w_n^1, w_n^2, \cdots, w_n^S \right]$ is a weight matrix composed of $w_n^i \left(i = 1, 2, \cdots, S \right)$.

2.2.4. High-Order Functional Connectivity

The methods mentioned earlier only captured low-level relationships of the brain in the spatial dimension. To simulate higher-order relationships between ROIs, Zhang *et al.* examined a method of constructing high-order BFNs (HOFC). Specifically, HOFC first calculates a BFN profile for each ROI and based on this BFN profile, a second layer of correlations is computed between all pairs of brain regions.

In recent years, numerous approaches have emerged for estimating BFNs through the use of various data-fitting terms and incorporating priors on BFN topology. These methods can generally be classified within a matrix-regularized framework [19]. For a more comprehensive understanding, it is recommended to consult a recent review [20] that extensively discusses the specific details and intricacies of these methodologies.

2.3. Proposed Model

We have mentioned several popular methods for constructing BFNs in Section 2.2. Despite their popularity, these methods for constructing BFNs can only model low-order relationships between ROIs. Although some methods have been proposed for constructing high-order BFN, the BFN they construct only

utilizes the spatial relationships between ROIs (such as the whole-correlation relationship characterized by PC, the partial-correlation relationship characterized by SR), while ignoring the temporal features of rs-fMRI features. To address this problem, We propose a method to construct high-order BFNs that takes into account both the spatial and temporal features of rs-fMRI signals. As shown in Figure 1, we presented our model that comprises spatial and temporal feature extraction layers, as well as high-order network construction layers.

2.3.1. Temporal Feature Extraction Module

To obtain more stable features of rs-fMRI signals in the temporal dimension, we performed a difference operation on it and the specific operation is as follows:

$$\Delta k_t = k_t - k_{t-1}, t = 2,3,\cdots,T \tag{7}$$

where k_t represents the signals of all ROIs at the n-th time point. By performing the above operations, we obtain $X = \left[\Delta k_1, \Delta k_2, \cdots, \Delta k_t, \cdots, \Delta k_{t-1}, \Delta k_T\right]$, which we regard as features along the time dimension. Subsequently, these features will be used to construct high-order temporal features of the BFN through $\otimes$ operation (*i.e.*, PC, SR, GSR).

2.3.2. Spatial Feature Extraction Module

In Figure 1, we depict the special relationships of ROIs. For i-th ROI, this type of relationship description refers to the relationship between i-th ROI and other

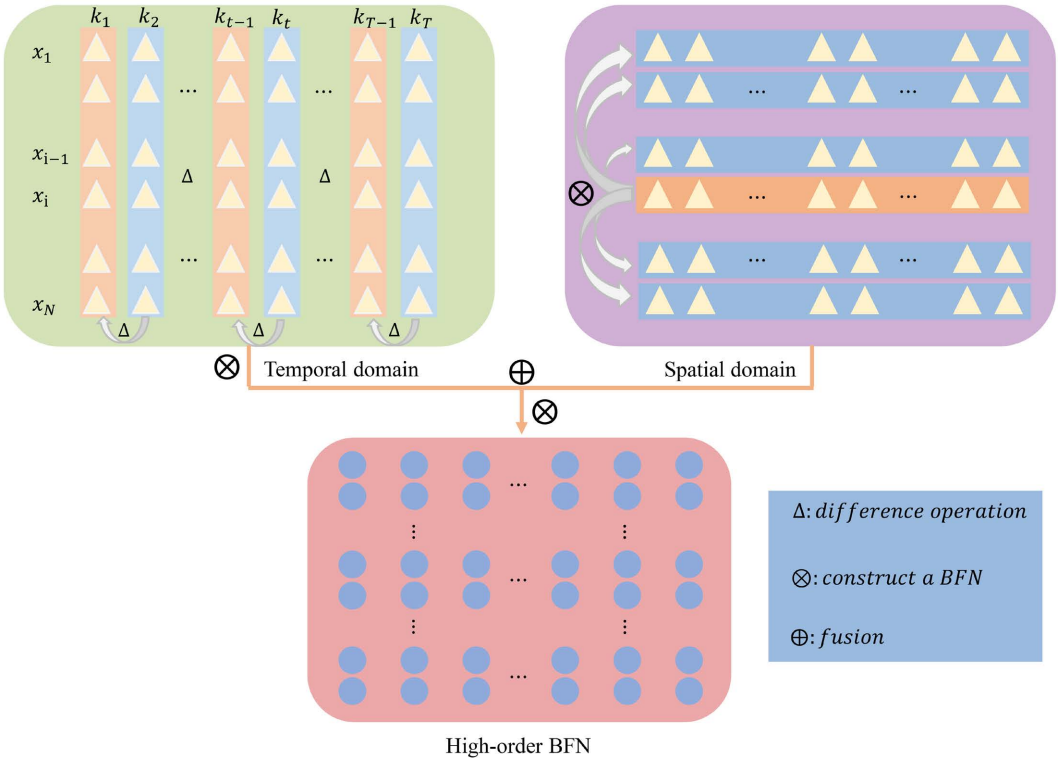

Figure 1. The high-order BFN construction module consists of three components: the spatial feature extraction module in the upper left corner, the temporal feature extraction module in the upper right corner, and the high-order BFN that fuses the features from both dimensions at the bottom.

ROIs ($n=1,\cdots,i-1,i+1,\cdots,N$). Similarly, we use $\otimes$ operations to characterize this spatial relationship (such as PC, SR, GSR).

2.3.3. High-Order BFN Construction Module

The input of this module consists of features in both the temporal and spatial dimensions. These features will be fused to construct a high-order BFN ($\oplus$) and we will discuss the impact of different fusion strategies on experimental results in Section 4.

3. Experiments and Results

3.1. Experimental Setting

In this work, we chose the two largest sites (*i.e.* NYU and UM) from the ABIDE dataset to confirm the efficacy of our method. Initially, we preprocessed the rs-fMRI data to obtain the BOLD signals from each subject, and later used these signals to construct BFNs. Due to the small sample size problem that exists in medical imaging fields, we have chosen to adopt the Leave-One-Out Cross-Validation (LOOCV) strategy to verify the proposed model. Specifically, for NYU dataset, containing 184 subjects, 183 of them are used for training while the remaining one is used for testing. As mentioned in Section 2.3, different methods can be employed to obtain the spatial domain features of the $\otimes$ operation, and this process involves some regularization parameters. In this paper, we adopt three different strategies for obtaining spatial features (*i.e.*, PC, SR, GSR). The regularization parameters involved in the BFN estimation models can affect the structure of the BFNs and the final classification result. To obtain the optimal parameters of each method, an inner LOOCV is further conducted on the training data to obtain the optimal parameters.

Once we obtain the BFNs of all subjects, the subsequent task is to differentiate between subjects with ASD and healthy control based on the estimated BFNs. For the identification task in our experiment, we utilize the edge weights of the BFNs as features. In particular, each BFN has 116 ROIs, producing $116\times(116-1)=13340$ features. This indicates that the feature dimension is much larger than the sample size (*i.e.*, the number of subjects), which not only brings about expensive computation, but also has the potential to negatively impact classification accuracy due to the so-called curse of dimensionality. To alleviate this situation, researchers have proposed many methods for feature selection such as t-test, least absolute shrinkage and selection operator (lasso) [21], GA [22], sparse group least absolute shrinkage and selection operator (sgLASSO) [23] and so on. In this paper, we use the popular t-test method for feature selection, and set the p-value to 0.05 and in order to provide a more comprehensive assessment of the effectiveness of the proposed method, we have incorporated the sgLASSO as a benchmark for feature selection. Subsequently, these selected features will be used as the input for the SVM classifier [24], which has been confirmed to work well in BFN-based classification tasks, to distinguish between normal controls and ASDs. Refer to **Figure 2** for a detailed demonstration of the steps.

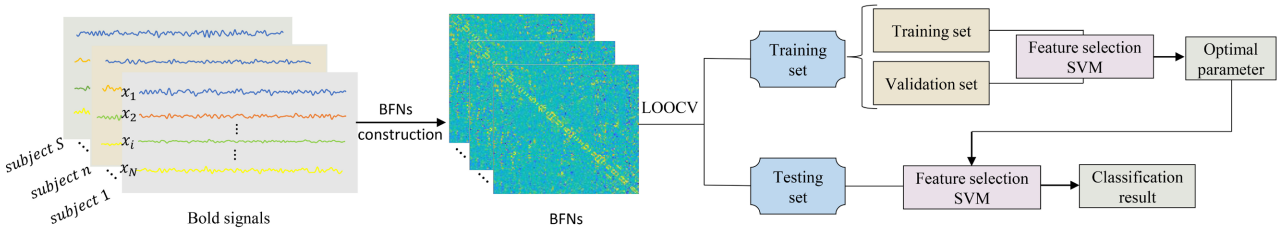

Figure 2. The main pipeline of ASD identification used in this study.

3.2. Compared Methods

In our experiments, we chose three classic methods for building BFN as the baseline methods, including PC, SR and GSR. Similarly, we compared with some high-order methods in our experiment which we categorized as CC-based methods (e.g., PC + CC). Furthermore, we conducted a comparative analysis of our proposed method against state-of-the-art deep learning techniques in our experiment such as classical deep neural network (DNN) and graph convolutional network (GCN) [25].

3.2.1. PC, SR, GSR

For SR and GSR-based methods, which contain one hyperparameter (*i.e.*, λ), and we search within the range of $\left[2^{-5}, 2^{-4}, \cdots, 2^{5}\right]$ to obtain the optimal parameter value for estimating BFNs. It is important to note that the method of building BFN based on PC does not involve any parameters. In order to ensure fairness in comparison and improve its flexibility, we have included a threshold parameter in PC to remove a proportion of weak edge weights in the estimated BFN.

3.2.2. High-Order Methods

In this work, we employ three high-order methods to construct BFN. For CC-based methods, to ensure comparability, the BFN construction parameters were kept consistent with those used in Section 3.2.1. This class of methods builds a BFN based on two identical operations. Taking PC as an example, we first use it to construct a low-order BFN. Then, we treat the constructed network as an adjacency matrix and use PC to construct a high-order BFN based on the adjacency matrix. In our study, in addition to using the CC-based method, we also compared our method to the current state-of-the-art approaches for constructing high-order BFN [HoFN_cope [15]]. This method contains two hyperparameters, which we kept consistent with their settings in our experiments.

3.2.3. DNN, GCN

For DNN, the input to the network is based on the PC-based BFN, which is a vectorized form of the network adjacency matrix. This is followed by two fully-connected hidden layers, consisting of 64 and 32 units respectively, with ReLU as the activation function in each layer. Finally, a softmax layer is used to identify ASD from normal controls. In the case of GCN, we also use the FCNs built by PC as network inputs, and set the absolute value of the FCNs to be initial node features. After two convolutional layers with ReLU activation functions,

the node features are mapped (via a readout operation) to a softmax layer through two fully-connected hidden layers, consisting of 64 and 32 units respectively.

3.3. Results

In order to evaluate the effectiveness of different methods, seven quantitative metrics including accuracy (ACC), sensitivity (SEN), specificity (SPE), balance accuracy (BAC), positive predictive value (PPV), negative predictive value (NPV) and area under Receiver Operating Characteristics (ROC) curve (AUC) are used to evaluate the performance of the model. The definitions of these metrics are given as follows:

$$\mathrm{ACC} = \frac{\mathrm{TP} + \mathrm{TN}}{\mathrm{TP} + \mathrm{TN} + \mathrm{FP} + \mathrm{FN}} \tag{8}$$

$$\mathrm{SEN} = \frac{\mathrm{TP}}{\mathrm{TP} + \mathrm{FN}} \tag{9}$$

$$\mathrm{SPE} = \frac{\mathrm{TN}}{\mathrm{TN} + \mathrm{FP}} \tag{10}$$

$$\mathrm{BAC} = \frac{\mathrm{SEN} + \mathrm{SPE}}{2} \tag{11}$$

$$\mathrm{PPV} = \frac{\mathrm{TP}}{\mathrm{TP} + \mathrm{FP}} \tag{12}$$

$$\mathrm{NPV} = \frac{\mathrm{TN}}{\mathrm{TN} + \mathrm{FN}} \tag{13}$$

where TP, TN, FP and FN denote the true positive, true negative, false positive, false negative, respectively. Of note, in this paper, we treat the ASD samples as a positive class while the normal control is as negative class.

In Table 2, the classification performance based on different methods is displayed, showcasing the corresponding ROC curves in Figure 3. The experimental results indicate that the proposed method outperforms the baseline methods. One possible reason is that the BFN we constructed is a high-order BFN, which can better capture the more complex interactive information between ROIs.

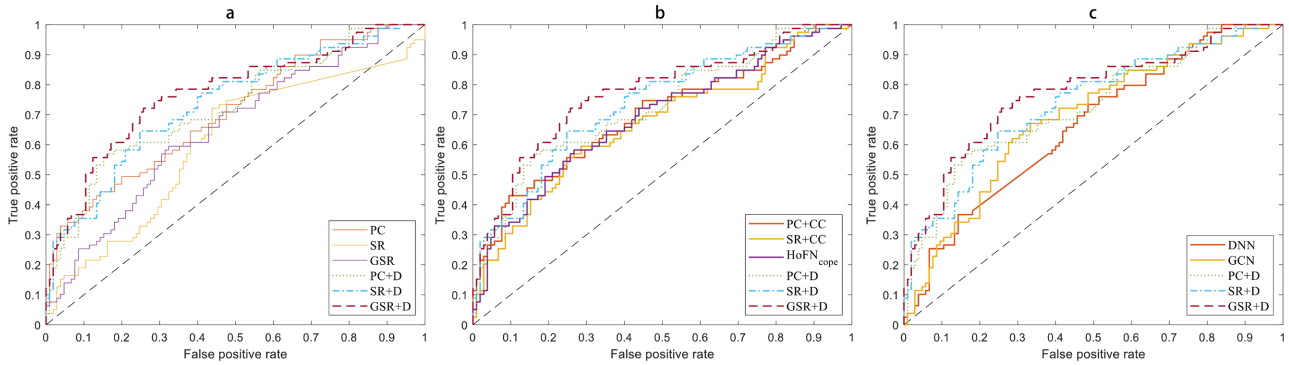

Figure 3. Panel (a) shows the comparison between our method and three baseline low-order BFN construction methods. Panel (b) shows the comparison between our method and three high-order BFN construction methods. Panel (c) shows the comparison between our method and two popular deep learning methods.

Table 2. Performance of different methods in NYU site of the ABIDE dataset.

Method	ACC	SEN	SPE	BAC	PPV	NPV	AUC
PC	63.04%	51.90%	71.42%	61.66%	57.75%	66.37%	70.54%
SR	55.98%	34.18%	72.38%	53.28%	48.21%	49.35%	62.98%
GSR	61.41%	48.10%	71.43%	59.77%	55.88%	64.66%	65.14%
PC + CC	64.67%	56.96%	70.48%	63.72%	59.21%	68.51%	69.63%
SR + CC	64.67%	49.37%	76.19%	62.78%	60.94%	66.67%	66.96%
HoFN_cope	67.39%	49.36%	80.95%	65.16%	66.10%	68.00%	68.99%
DNN	63.04%	37.97%	81.90%	59.94%	61.22%	63.70%	66.17%
GCN	64.13%	49.37%	75.24%	62.30%	60.00%	66.39%	68.97%
PC + D	69.57%	60.76%	76.19%	68.48%	65.75%	72.07%	72.53%
SR + D	71.20%	64.56%	76.19%	70.37%	67.11%	74.07%	78.05%
GSR + D	71.74%	67.09%	75.24%	71.16%	67.09%	75.24%	77.18%

Another factor that may have contributed to our good performance is that the high-order BFN we built takes into account both temporal and spatial features.

To further validate the efficacy of the proposed model, we conduct an ASD vs. NC classification experiment on the UM site of the ABIDE dataset. The experimental results, as shown in Table 3, demonstrate that the proposed method outperforms the baseline methods in terms of accuracy, sensitivity, and specificity. These findings clearly showcase the superiority of the proposed method. We attribute this improved performance to our ability to construct a BFN that efficiently captures complex information and accurately reflects the subtle variations in the brain, which leads to a more effective classification outcome.

4. Discussion

4.1. Hyper-Parameter Selection

The hyper-parameter involved in the BFN estimation models may affect the structure of the BFNs and the final classification result. We explore the impact of selecting different hyper-parameter (*i.e.*, λ) values on the performance of the experiment [26] [27]. It is noteworthy that, in this study, we employ two feature selection methods, t-test and sgLASSO, to investigate the influence of various thresholds or hyper-parameter on the experimental performance. As shown in Figure 4, regardless of which feature selection method we choose, our method generally outperforms the baseline method in most cases. In addition, compared to the baseline method, the proposed model has a small performance variation when selecting different hyper-parameter values, meaning that it performs more steadily.

4.2. Discriminative Features

In addition to the accuracy of ASD classification itself, there is an interesting

Table 3. Performance of different methods in UM site of the ABIDE dataset.

Method	ACC	SEN	SPE	BAC	PPV	NPV	AUC
PC	63.45%	63.24%	63.64%	63.44%	62.32%	68.70%	66.10%
SR	64.14%	54.41%	72.73%	63.57%	63.79%	64.37%	75.63%
GSR	60.69%	61.76%	59.74%	59.77%	56.79%	65.63%	63.90%
PC + CC	63.45%	60.29%	66.23%	63.26%	61.19%	65.38%	68.71%
SR + CC	68.97%	60.29%	76.62%	68.46%	69.49%	68.60%	73.87%
HoFN_cope	63.45%	57.35%	68.83%	63.09%	61.90%	64.63%	66.92%
DNN	60.69%	52.94%	67.53%	60.23%	59.02%	61.90%	67.65%
GCN	64.83%	66.18%	63.64%	64.91%	61.64%	68.06%	74.16%
PC + D	73.10%	69.12%	76.62%	68.48%	65.75%	72.07%	72.53%
SR + D	71.03%	66.18%	75.32%	70.75%	70.31%	71.60%	76.07%
GSR + D	71.72%	63.24%	79.22%	71.23%	72.88%	70.93%	74.52%

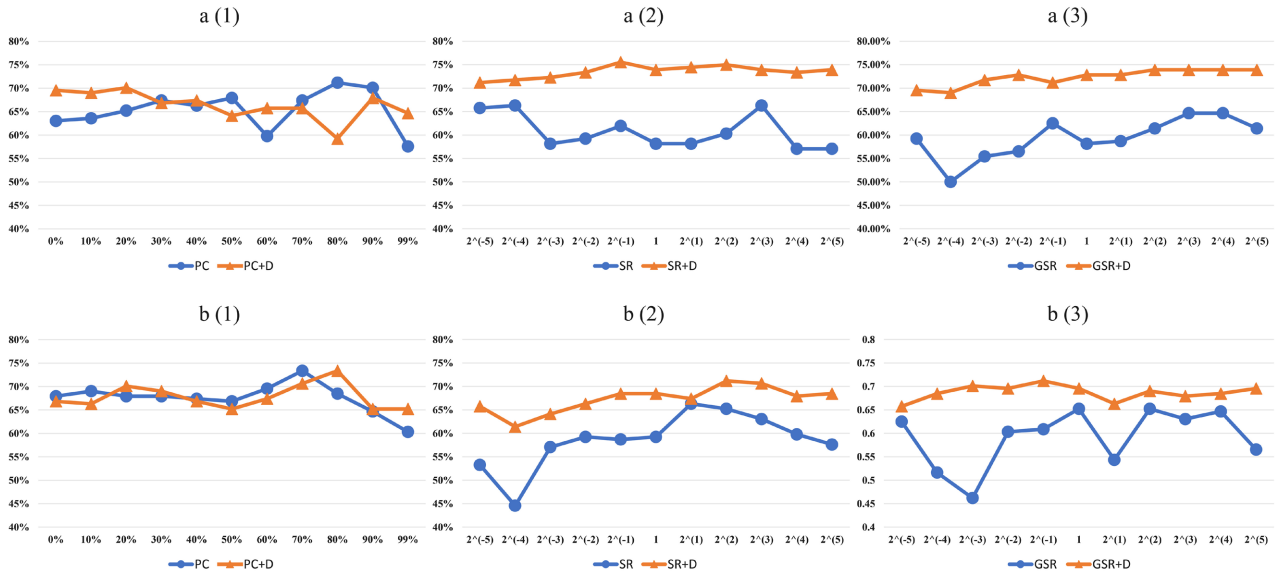

Figure 4. a(1)-a(3) represents the impact of the regularization parameter on the performance of different methods when t-test feature selection is applied, while b(1)-b(3) demonstrates the impact of the regularization parameter on the performance of different methods when sgLASSO feature selection is applied.

question of which features (*i.e.*, functional connections or corresponding ROIs in BFNs) contribute the most to the recognition of specific disease identification tasks. In this experiment, we first selected 21 most distinctive features (with a p-value of 0.0005) that were most relevant to the ASD classification task, and visualized them separately in **Figure 5**.

Specifically, each arc in **Figure 5** displays the selected features between two ROIs. The thickness of each arc represents its discriminative power inversely proportional to the corresponding p-value. As we can see, the first few significant brain regions include the hippocampus, parahippocampal gyrus, and amygdala. This is consistent with recent studies [28] [29] [30] [31].

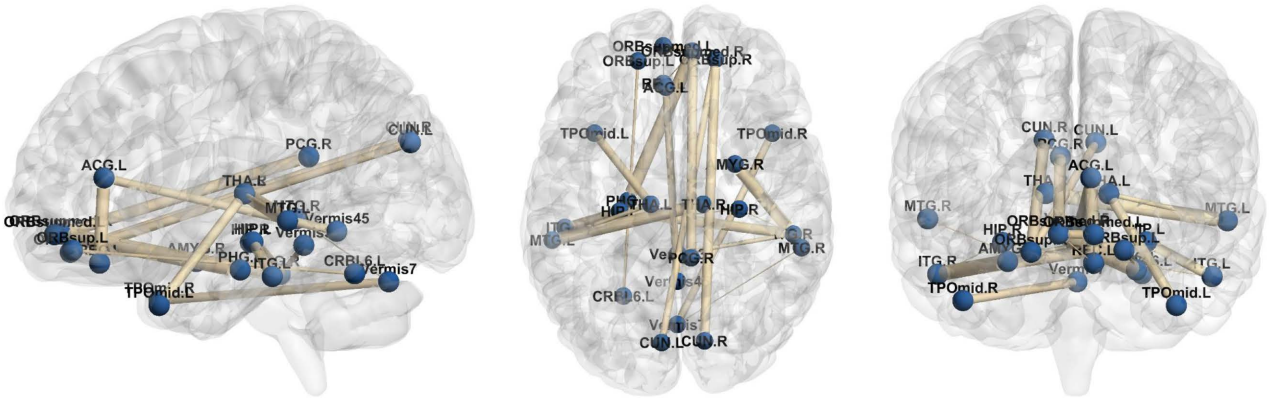

Figure 5. The discriminative features with t-test selection are identified for ASD classification. Each arc in the figure displays the selected feature between two ROIs, where the thickness indicates its discriminative power for classification.

4.3. Parameter Analysis

When performing feature selection using t-tests, the size of the p-value directly affects the number of selected features, which in turn has a significant impact on the experimental results. In our experiment, we conducted feature selection using p-values of 0.005 and 0.1. As shown in **Figure 6**, using different p-value can indeed have an impact on experimental results, but our proposed method demonstrated better performance compared to the baseline method. This improvement may be attributed to our construction of a high-order BFN that more accurately reflects the true state of the brain and thus improves our classification performance.

4.4. The Impact of Differentiation

In this paper, we encode the temporal features of ROIs through differential operation. In this section, we discuss the impact of the degree of differentiation on the experimental performance. Take GSR + D as an example, if we do not perform differential operation, our model will be a classic GSR model, corresponding to $D = 0$ in **Figure 7**. As we can see, when the high-order difference $D < 6$ is used, our experimental performance is higher than the baseline GSR because appropriate differentiation can fully encode the BOLD signal's temporal features. However, when $D > 15$, our experimental performance exhibits lower performance, possibly because the high degree of differentiation can increase the signal noise and enhance the signal oscillation, weakening or attenuating certain signal features and thereby affecting the overall model performance [32] [33].

4.5. Fusion Strategies

Different fusion strategies ($\oplus$) have a certain impact on the final experimental performance. Concatenation ($\|$) and summation ($\odot$) are the simplest and most effective fusion strategies that have been successfully applied to three-dimensional shape recognition [34]. **Table 4** presents the experimental performance of the PC-based, SR-based and GSR-based BFN construction method under the influence

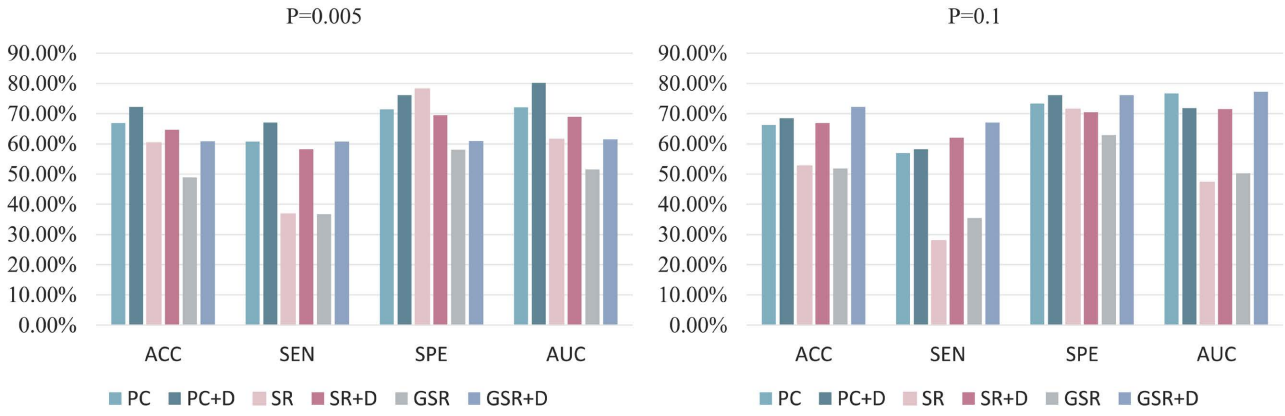

Figure 6. The impact of selecting different P values on experimental results.

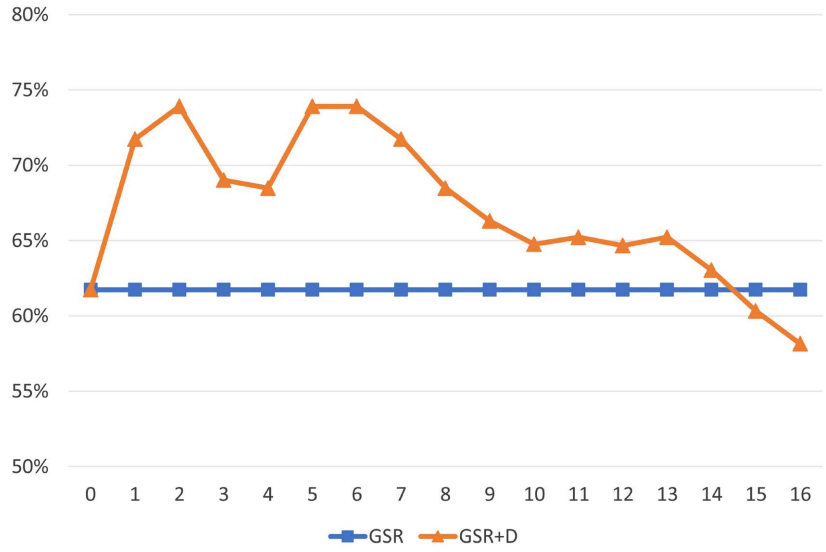

Figure 7. The impact of various degrees of differentiation on experimental performance. The blue line represents the experimental performance without differentiation, while the orange line represents the influence of the degree of differentiation on the experimental performance.

Table 4. The experimental results were obtained using different fusion strategies on the UM site.

Methods	ACC	SEN	SPE	AUC
PC + D (⊕)	73.10%	69.12%	76.62%	72.53%
PC + D (⊙)	71.72%	67.65%	75.32%	78.76%
SR + D (⊕)	71.03%	66.18%	75.32%	76.07%
SR + D (⊙)	75.17%	70.59%	79.22%	84.80%
GSR + D (⊕)	71.72%	63.24%	79.22%	74.52%
GSR + D (⊙)	71.03%	63.24%	77.92%	77.85%

of these two fusion strategies. The experimental results demonstrate that different fusion strategies have an impact on the experimental performance. Overall,

both strategies exhibit high experimental performance, and a suitable fusion approach can enhance the final experimental performance to a certain extent.

5. Conclusion

This paper proposes a novel high-order brain functional network (BFN) construction scheme that encodes the relationships between ROIs in both spatial and temporal dimensions, resulting in a BFN that accurately reflects the true state of the brain. Although the proposed method performs better than the baseline methods, it has certain limitations. For example, it is limited to transductive models and lacks strong generalization capabilities. In our future work, we will consider utilizing a deep learning framework to design an end-to-end model that enhances the generalization performance of the constructed model.

Conflicts of Interest

The authors declare no conflicts of interest regarding the publication of this paper.

References

[1] Mohamed, F.E.B., Zaky, E.A., El-Sayed, A.B., Elhossieny, R.M., Zahra, S.S., Salah Eldin, W., Youssef, W.Y., Khaled, R.A. and Youssef, A.M. (2015) Assessment of Hair Aluminum, Lead, and Mercury in a Sample of Autistic Egyptian Children: Environmental Risk Factors of Heavy Metals in Autism. *Behavioural Neurology*, **2015**, Article ID: 545674. https://doi.org/10.1155/2015/545674

[2] Osredkar, J., Gosar, D., Maček, J., Kumer, K., Fabjan, T., Finderle, P., Šterpin, S., Zupan, M. and Jekovec Vrhovsek, M. (2019) Urinary Markers of Oxidative Stress in Children with Autism Spectrum Disorder (ASD). *Antioxidants*, **8**, Article No. 187. https://doi.org/10.3390/antiox8060187

[3] Simonoff, E., Pickles, A., Charman, T., Chandler, S., Loucas, T. and Baird, G. (2008) Psychiatric Disorders in Children with Autism Spectrum Disorders: Prevalence, Comorbidity, and Associated Factors in a Population-Derived Sample. *Journal of the American Academy of Child & Adolescent Psychiatry*, **47**, 921-929. https://doi.org/10.1097/CHI.0b013e318179964f

[4] Maenner, M.J., Shaw, K.A., Bakian, A.V., Bilder, D.A., Durkin, M.S., Esler, A., Furnier, S.M., Hallas, L., Hall-Lande, J., Hudson, A., *et al.* (2021) Prevalence and Characteristics of Autism Spectrum Disorder Among Children Aged 8 Years—Autism and Developmental Disabilities Monitoring Network, 11 Sites, United States, 2018. *MMWR Surveillance Summaries*, **70**, 1-16. https://doi.org/10.15585/mmwr.ss7011a1

[5] Buckner, R.L., Krienen, F.M. and Yeo, B.T. (2013) Opportunities and Limitations of Intrinsic Functional Connectivity MRI. *Nature Neuroscience*, **16**, 832-837. https://doi.org/10.1038/nn.3423

[6] Li, Y., Liu, J., Tang, Z. and Lei, B. (2020) Deep Spatial-Temporal Feature Fusion from Adaptive Dynamic Functional Connectivity for MCI Identification. *IEEE Transactions on Medical Imaging*, **39**, 2818-2830. https://doi.org/10.1109/TMI.2020.2976825

[7] Van Den Heuvel, M.P. and Pol, H.E.H. (2010) Exploring the Brain Network: A Review on Resting-State fMRI Functional Connectivity. *European Neuropsychophar-*

macology, **20**, 519-534. https://doi.org/10.1016/j.euroneuro.2010.03.008

[8] Fornito, A., Zalesky, A. and Breakspear, M. (2015) The Connectomics of Brain Disorders. *Nature Reviews Neuroscience*, **16**, 159-172. https://doi.org/10.1038/nrn3901

[9] Smith, S.M., Vidaurre, D., Beckmann, C.F., Glasser, M.F., Jenkinson, M., Miller, K.L., Nichols, T.E., Robinson, E.C., Salimi-Khorshidi, G., Woolrich, M.W., *et al.* (2013) Functional Connectomics from Resting-State fMRI. *Trends in Cognitive Sciences*, **17**, 666-682. https://doi.org/10.1016/j.tics.2013.09.016

[10] Peng, J., Wang, P., Zhou, N. and Zhu, J. (2009) Partial Correlation Estimation by Joint Sparse Regression Models. *Journal of the American Statistical Association*, **104**, 735-746. https://doi.org/10.1198/jasa.2009.0126

[11] Wee, C.-Y., Yap, P.-T., Zhang, D., Wang, L. and Shen, D. (2014) Group- Constrained Sparse fMRI Connectivity Modeling for Mild Cognitive Impairment Identification. *Brain Structure and Function*, **219**, 641-656. https://doi.org/10.1007/s00429-013-0524-8

[12] Zhao, F., Zhang, H., Rekik, I., An, Z. and Shen, D. (2018) Diagnosis of Autism Spectrum Disorders Using Multi-Level High-Order Functional Networks Derived From Resting-State Functional MRI. *Frontiers in Human Neuroscience*, **12**, Article 184. https://doi.org/10.3389/fnhum.2018.00184

[13] Zhang, H., Chen, X., Shi, F., Li, G., Kim, M., Giannakopoulos, P., Haller, S. and Shen, D. (2016) Topographical Information-Based High-Order Functional Connectivity and Its Application in Abnormality Detection for Mild Cognitive Impairment. *Journal of Alzheimer's Disease*, **54**, 1095-1112. https://doi.org/10.3233/JAD-160092

[14] Chen, X., Zhang, H., Gao, Y., Wee, C. Y., Li, G., Shen, D. and Alzheimer's Disease Neuroimaging Initiative (2016) High-Order Resting-State Functional Connectivity Network for MCI Classification. *Human Brain Mapping*, **37**, 3282-3296. https://doi.org/10.1002/hbm.23240

[15] Su, H., Zhang, L., Qiao, L. and Liu, M. (2022) Estimating High-Order Brain Functional Networks by Correlation-Preserving Embedding. *Medical & Biological Engineering & Computing*, **60**, 2813-2823. https://doi.org/10.1007/s11517-022-02628-7

[16] Yan, C.-G., Wang, X.-D., Zuo, X.-N. and Zang, Y.-F. (2016) DPABI: Data Processing & Analysis for (Resting-State) Brain Imaging. *Neuroinformatics*, **14**, 339-351. https://doi.org/10.1007/s12021-016-9299-4

[17] Tzourio-Mazoyer, N., Landeau, B., Papathanassiou, D., Crivello, F., Etard, O., Delcroix, N., Mazoyer, B. and Joliot, M. (2002) Automated Anatomical Labeling of Activations in SPM Using a Macroscopic Anatomical Parcellation of the MNI MRI Single-Subject Brain. *Neuroimage*, **15**, 273-289. https://doi.org/10.1006/nimg.2001.0978

[18] Li, W., Wang, Z., Zhang, L., Qiao, L. and Shen, D. (2017) Remodeling Pearson's Correlation for Functional Brain Network Estimation and Autism Spectrum Disorder Identification. *Frontiers in Neuroinformatics*, **11**, Article 55. https://doi.org/10.3389/fninf.2017.00055

[19] Qiao, L., Zhang, H., Kim, M., Teng, S., Zhang, L. and Shen, D. (2016) Estimating Functional Brain Networks by Incorporating a Modularity Prior. *Neuroimage*, **141**, pp. 399-407. https://doi.org/10.1016/j.neuroimage.2016.07.058

[20] Qiao, L., Zhang, L., Chen, S. and Shen, D. (2018) Data-Driven Graph Construction and Graph Learning: A Review. *Neurocomputing*, **312**, 336-351. https://doi.org/10.1016/j.neucom.2018.05.084

[21] Tibshirani, R. (1996) Regression Shrinkage and Selection via the Lasso. *Journal of the Royal Statistical Society*: *Series B* (*Methodological*), **58**, 267-288.

https://doi.org/10.1111/j.2517-6161.1996.tb02080.x

[22] Szenkovits, A., Meszlényi, R., Buza, K., Gaskó, N., Lung, R.I. and Suciu, M. (2018) Feature Selection with a Genetic Algorithm for Classification of Brain Imaging Data. In: Stańczyk, U., Zielosko, B. and Jain, L., Eds., *Advances in Feature Selection for Data and Pattern Recognition*. *Intelligent Systems Reference Library*, Vol. 138, Springer, Cham, 185-202. https://doi.org/10.1007/978-3-319-67588-6_10

[23] Jiang, X., Qiao, L., De Leone, R. and Shen, D. (2022) Joint Selection of Brain Network Nodes and Edges for MCI Identification. *Computer Methods and Programs in Biomedicine*, **225**, Article ID: 107082. https://doi.org/10.1016/j.cmpb.2022.107082

[24] Chang, C.-C. and Lin, C.-J. (2011) LIBSVM: A Library for Support Vector Machines. *ACM Transactions on Intelligent Systems and Technology* (*TIST*), **2**, 1-27. https://doi.org/10.1145/1961189.1961199

[25] Kipf, T.N. and Welling, M. (2016) Semi-Supervised Classification with Graph Convolutional Networks. ArXiv Preprint ArXiv: 1609.02907.

[26] Jiang, X., Zhang, L., Qiao, L. and Shen, D. (2019) Estimating Functional Connectivity Networks via Low-Rank Tensor Approximation with Applications to MCI Identification. *IEEE Transactions on Biomedical Engineering*, **67**, 1912-1920. https://doi.org/10.1109/TBME.2019.2950712

[27] Xue, Y., Zhang, L., Qiao, L. and Shen, D. (2020) Estimating Sparse Functional Brain Networks with Spatial Constraints for MCI Identification. *PLOS ONE*, **15**, e0235039. https://doi.org/10.1371/journal.pone.0235039

[28] Chaddad, A., Desrosiers, C., Hassan, L. and Tanougast, C. (2017) Hippocampus and Amygdala Radiomic Biomarkers for the Study of Autism Spectrum Disorder. *BMC Neuroscience*, **18**, Article No. 52. https://doi.org/10.1186/s12868-017-0373-0

[29] Del Casale, A., Ferracuti, S., Alcibiade, A., Simone, S., Modesti, M.N. and Pompili, M. (2022) Neuroanatomical Correlates of Autism Spectrum Disorders: A Meta-Analysis of Structural Magnetic Resonance Imaging Studies. *Psychiatry Research*: *Neuroimaging*, **325**, Article ID: 111516. https://doi.org/10.1016/j.pscychresns.2022.111516

[30] Glerean, E., Pan, R. K., Salmi, J., Kujala, R., Lahnakoski, J. M., Roine, U., Nummenmaa, L., Leppämäki, S., Nieminen-von Wendt, T., Tani, P., *et al.* (2016) Reorganization of Functionally Connected Brain Subnetworks in High-Functioning Autism. *Human Brain Mapping*, **37**, 1066-1079. https://doi.org/10.1002/hbm.23084

[31] Zhang, C., Ma, Y., Qiao, L., Zhang, L. and Liu, M. (2023) Learning to Fuse Multiple Brain Functional Networks for Automated Autism Identification. *Biology*, **12**, Article No. 971. https://doi.org/10.3390/biology12070971

[32] Ramsey, J.D., Hanson, S.J., Hanson, C., Halchenko, Y.O., Poldrack, R.A. and Glymour, C. (2010) Six Problems for Causal Inference from fMRI. *Neuroimage*, **49**, 1545-1558. https://doi.org/10.1016/j.neuroimage.2009.08.065

[33] Price, K., Storn, R.M. and Lampinen, J.A. (2006) Differential Evolution: A Practical Approach to Global Optimization. Springer Science & Business Media, Berlin.

[34] Su, H., Maji, S., Kalogerakis, E. and Learned-Miller, E. (2015) Multi-View Convolutional Neural Networks for 3D Shape Recognition. *Proceedings of the IEEE International Conference on Computer Vision*, Santiago, 7-13 December 2015, 945-953. https://doi.org/10.1109/ICCV.2015.114